# NACA

# RESEARCH MEMORANDUM

INVESTIGATION OF ROTATING-STALL LIMITS IN

A SUPERSONIC TURBOFAN ENGINE

By James F. Dugan, Jr.

Lewis Flight Propulsion Laboratory
Cleveland, Ohio

Declassified July 17, 1962

# NATIONAL ADVISORY COMMITTEE
# FOR AERONAUTICS
## WASHINGTON

October 3, 1957

4319

CU-1

NATIONAL ADVISORY COMMITTEE FOR AERONAUTICS

RESEARCH MEMORANDUM

INVESTIGATION OF ROTATING-STALL LIMITS IN

A SUPERSONIC TURBOFAN ENGINE

By James F. Dugan, Jr.

## SUMMARY

A theoretical mixed-jet one-spool turbofan engine was analyzed over a range of flight Mach numbers up to 2.95. The engine was characterized by an eight-stage fan-compressor unit. The compressor and fan performance maps were computed from experimentally determined stage data and a stage-stacking procedure. To supplement the analytical results, experimental tests were conducted on a rotor-blade row rigged to simulate first-stage operation of a turbofan engine.

The variation of the turbofan inlet flow coefficient with flight Mach number and the experimental results indicate that turbofan flow would probably be free of rotating stall.

## INTRODUCTION

The turbofan engine offers a potential method of avoiding the severe blade vibratory stresses excited by rotating stall that have plagued various turbojet engines. The rotating stall in these engines occurred whenever an engine was operated below some limiting value of equivalent speed (usually, in the range from 70 to 80 percent of design equivalent speed). Stator adjustment, interstage bleed, and inlet baffles have been used successfully in turbojet engines to remedy the excessive blade vibratory stresses caused by rotating stall (refs. 1 to 4). The use of a turbofan engine is another possible way of avoiding rotating-stall-excited blade vibratory stresses. If the fan operates near design flow conditions over a wide range of equivalent speed, tip-rotating stall (which is the most common type) will not occur.

In order to determine the operating limits for the occurrence of rotating stall, fan and compressor operation in a supersonic turbofan engine was investigated. In previous turbofan investigations, which were concerned mainly with engine performance (e.g., refs. 5 to 8), the fan performance map was considered to be that which would be obtained

from testing the fan as a separate component. In this investigation,
however, a different approximation of fan performance is desirable, be-
cause the radial variations of flow parameters ahead of and behind the
fan affect the phenomenon of rotating stall. For conventional axial-
flow compressors, rotating stall usually occurs initially at the blade
tips of the first stage. In the turbofan engine, the throttling at the
tip section of the first stage may be less severe than that at the root
section. This type of engine, then, may be less susceptible to the
occurrence of rotating stall.

A theoretical mixed-jet one-spool turbofan engine is analyzed here-
in over a range of flight Mach numbers up to 2.95. In addition, experi-
mental tests conducted on a rotor-blade row rigged to simulate first-
stage operation of a turbofan engine are described. The analytical
engine is characterized by an eight-stage fan-compressor unit. The fan
is composed of the outer annulus of stages 1 and 2, while the compressor
is composed of the inner annulus of stages 1 and 2, and stages 3 to 8.
The flow through the fan and compressor is idealized by considering an
imaginary shroud separating fan flow from compressor flow in the first
two stages. Fan and compressor performance maps are computed from the
interstage data of the NACA eight-stage compressor (ref. 9) and the stage-
stacking procedure of reference 10. Fan and compressor operating lines
are found by matching the turbofan-engine components for operation over
the whole flight range at the design values of mechanical speed and
turbine-inlet temperature.

## METHOD OF ANALYSIS

### Analytical Procedure

A cross section of the turbofan engine is presented in figure 1.
The imaginary shroud which separates fan flow from compressor flow is
shown by the dashed line between axial stations A and B. The fan con-
sists of the outer part of stages 1 and 2, while the compressor is com-
posed of the inner part of stages 1 and 2 and stages 3 to 8. At design
conditions, about 59 percent of the total airflow bypasses the compres-
sor, combustor, and turbine components. This value lies within the range
of interest for turbofan engines. A supersonic turbofan would have an
afterburner, but none is considered in this report, since engine per-
formance is not calculated. The presence or absence of an afterburner
does not affect the component matching required to establish full-power
operating lines on the fan and compressor performance maps.

Fan performance. - Turbofan fan performance was obtained by con-
structing generalized performance curves and then computing fan perform-
ance from the generalized curves and specified design information. The
generalized curves were obtained from eight-stage interstage data used

in preparing reference 9.  During the compressor tests (ref. 9), total-
pressure and total-temperature rakes were located behind stator blade
rows and between blade wakes.  The rakes had five measuring tips located
at centers of equal annular areas.  To obtain the generalized fan curves,
the data at the compressor inlet and behind the second stator were used.
The fan-exit total pressures and total temperatures were obtained by
arithmetically averaging the readings from the outer three rake measur-
ing tips.  Generalized fan performance curves were plotted as equivalent
total-temperature rise and equivalent total-pressure ratio against flow
coefficient.  These parameters are defined by the following equations
(all symbols are defined in the appendix):

$$\left(\frac{T_B - T_A}{T_A}\right)_{eq} = \left(\frac{T_B - T_A}{T_A}\right) \frac{\left(\frac{U_m}{\sqrt{\theta}}\right)^2_{A,d}}{\left(\frac{U_m}{\sqrt{\theta}}\right)^2_A} \tag{1}$$

$$\left(\frac{P_B}{P_A}\right)_{eq} = \left\{\left[\left(\frac{P_B}{P_A}\right)^{\frac{\gamma-1}{\gamma}} - 1\right] \frac{\left(\frac{U_m}{\sqrt{\theta}}\right)^2_{A,d}}{\left(\frac{U_m}{\sqrt{\theta}}\right)^2_A} + 1\right\}^{\frac{\gamma}{\gamma-1}} \tag{2}$$

$$\left(\frac{V_z}{U}\right)_{m,A} = \frac{f\left[\left(\frac{w\sqrt{\theta}}{\delta A_{an}}\right)_A, \beta_A\right]}{\left(\frac{U_m}{\sqrt{\theta}}\right)_A} \tag{3}$$

    The fan design information necessary to compute a fan performance
map resulted from assigned turbofan-engine design values.  The fan de-
sign equivalent tip speed was set equal to 1218 feet per second, which
is also the design equivalent tip speed of the modified eight-stage com-
pressor (ref. 10).  Other turbofan-engine design values were assigned
as follows:

Equivalent weight flow, lb/sec . . . . . . . . . . . . . . . . . . . . 100
Equivalent specific weight flow, (lb/sec)/sq ft . . . . . . . . . . 30
Inlet compressor-hub to fan-tip radius ratio . . . . . . . . . . . 0.46

The imaginary hub radius at the fan inlet, which is also the imaginary tip radius at the compressor inlet, was assigned to be the mean radius of the annulus at the turbofan inlet.

Turbofan fan design values are as follows:

Total-pressure ratio, $(P_B/P_A)_d$ . . . . . . . . . . . . . . . . . . . 1.95

Mean equivalent rotor speed, $(U_m/\sqrt{\theta})_{A,d}$, ft/sec . . . . . . . . 1054

Equivalent weight flow, $(w\sqrt{\theta}/\delta)_{A,d}$, lb/sec . . . . . . . . . . 59.25

Tip relative Mach number, $M'_{t,A,d}$ . . . . . . . . . . . . . . . 1.237

Annulus area at fan inlet, $A_{an,A}$, sq ft . . . . . . . . . . . . 1.557

Adiabatic efficiency, $\eta_{f,d}$ . . . . . . . . . . . . . . . . . . . . 0.874

Compressor performance. - The turbofan compressor map was computed from generalized stage curves, design information, and the stage-stacking procedure discussed in reference 10. The generalized curves for compressor stages 1 and 2 in combination were obtained from the eight-stage interstage data used in preparing reference 9. The total pressures and total temperatures at the exit of stage 2 were obtained by arithmetically averaging the readings from the inner three rake measuring tips. Generalized performance curves for compressor stages 1 and 2 were plotted as equivalent total-temperature rise and equivalent total-pressure ratio against flow coefficient. The generalized performance curves of compressor stages 3 to 8 are the same as those of stages 3 to 8 in reference 10.

Turbofan compressor design values are as follows:

Total-pressure ratio, $(P_2/P_1)_d$ . . . . . . . . . . . . . . . . . . 8.45

Equivalent weight flow, $(w\sqrt{\theta}/\delta)_{1,d}$, lb/sec . . . . . . . . . . 40.75

Adiabatic efficiency, $\eta_{c,d}$ . . . . . . . . . . . . . . . . . . . 0.874

Mean equivalent rotor speed, $(U_m/\sqrt{\theta})_{1,d}$, ft/sec . . . . . . . . 724.7

Annulus area at compressor inlet, $A_{an,1}$, sq ft . . . . . . . . . 1.071

Tip relative Mach number, $M'_{t,1,d}$, . . . . . . . . . . . . . . . 0.974

The values of annulus area ratio, mean-radius ratio, and absolute flow angle needed to compute compressor performance by the stage-stacking technique (ref. 10) are listed in the following table:

| Stage | Annulus area ratio, $\dfrac{A_{an,n-1}}{A_{an,n}}$ | Mean-radius ratio, $\dfrac{r_{m,n}}{r_{m,n-1}}$ | Absolute flow angle, $\beta_n$, deg |
|-------|------|------|-----|
| 1 & 2 | ----- | ----- | 0 |
| 3 | 1.304 | 1.246 | 30 |
| 4 | 1.370 | 1.030 | 30 |
| 5 | 1.152 | 1.010 | 30 |
| 6 | 1.174 | 1.010 | 30 |
| 7 | 1.184 | 1.008 | 30 |
| 8 | 1.145 | 1.006 | 30 |

Combustor performance. - Combustor efficiency and total-pressure ratio were assigned to be constant for all operating conditions:

Combustor efficiency, $\eta_{2,3}$ . . . . . . . . . . . . . . . . . . . . . . . . . . . . 0.95

Combustor total-pressure ratio, $P_3/P_2$ . . . . . . . . . . . . . . . 0.94

Turbine performance. - Several simplifying assumptions are made regarding turbine performance. The equivalent weight flow at the turbine inlet is assumed constant for all operating conditions. The turbine efficiency is assumed to vary according to the following equation, which is a development of the efficiency parabola discussed on page 222 of reference 11.

$$\eta_{3,4} = a + b \left( \frac{\frac{N}{\sqrt{\theta_3}}}{\sqrt{\frac{H_3 - H_4}{\theta_3}}} - c \right)^2 \tag{4}$$

where

a     design value of turbine efficiency, 0.85

b     $-a/c^2$

c     design value of $(N/\sqrt{\theta_3})/\sqrt{(H_3 - H_4)/\theta_3}$

Turbine efficiency in the turbofan engine varied from 0.83 to 0.85 for the range of operation considered.

Component matching. - Fan and compressor operating lines were calculated from the assigned flight conditions, the assigned mode of engine operation, component performance, and a component matching procedure.

Flight conditions were specified by flight Mach number and altitude. For full-power operation in the stratosphere, flight Mach number varied from 1.28 to 2.95. The values of turbofan mechanical speed and turbine-inlet temperature were held fixed at their design values for all flight conditions.

Before the component matching procedure could be used, turbofan constants had to be calculated or assigned. The annulus area at station 5 (see fig. 1) was sized to give a design Mach number at this station equal to 0.2. The annulus area at station C was sized to satisfy the condition that $p_C = p_5$ at design conditions. The area at station 6 was set equal to the sum of the flow area at stations 5 and C. Duct total-pressure ratio $P_C/P_B$ was assigned to be 0.97.

For a specified flight condition and mode of engine operation, the compressor operating point was found by satisfying the following equation:

$$\frac{w_1\sqrt{\theta_1}}{\delta_1}\frac{\sqrt{\frac{T_3}{T_1}}}{\frac{P_2}{P_1}} = \frac{w_1\sqrt{\theta_3}}{\delta_2} = \left(\frac{w_1\sqrt{\theta_3}}{\delta_2}\right)_d \qquad (5)$$

Equation (5) implies that the fuel-air ratio, as well as combustor total-pressure ratio and turbine-inlet equivalent weight flow, is constant.

The fan operating point is found by iteration. A trial fan operating point is assigned along the known equivalent-speed line $(N/\sqrt{\theta})_A$. The static pressure is calculated at station C, where axial flow is assumed to exist. A turbine operating point is calculated for the known compressor operating point and the trial fan operating point by using the condition that fan power plus compressor power equals turbine power. The static pressure is also calculated at station 5, where axial flow is assumed. If $p_5$ does not equal $p_C$, a second trial fan operating point is assigned. The iteration is repeated until $p_5$ equals $p_C$, thereby fixing the correct fan and turbine operating points.

### Experimental Procedure

The inlet flow coefficient below which rotating stall exists in the turbofan engine is probably influenced by the condition of separate throttling in the outer and inner annuli. In order to investigate this probability, a rotor-blade row was run at conditions simulating turbofan operation. The annulus behind the blade row was divided into two annuli by a cylindrical shell. The diameter of the shell was equal to the arithmetic mean of the inner and outer diameters of the total annulus.

A strip of rubber was clamped to the inner surface of the inner annulus. By regulating the air pressure beneath the rubber strip, additional throttling in the inner annulus could be achieved. The rotor was first operated at 60-percent design speed with no additional throttling in the inner annulus. The airflow was decreased until the presence of rotating stall was detected by means of hot-wire anemometers. The rotor was then operated with various amounts of additional throttling in the inner annulus. Again, the speed was held constant while the airflow was decreased until rotating stall was detected.

In order to learn how the flow readjusted when more flow than normal was forced through the outer annulus, flow ahead of and behind the rotor was measured during operation with and without additional throttling in the inner annulus downstream of the rotor.

## RESULTS AND DISCUSSION

### Performance Maps

The turbofan fan performance is shown in figure 2. Figure 2(a) shows the generalized performance curves that resulted from data used in preparing reference 9. Figure 2(b) is the fan performance map obtained from the generalized curves and specified design values.

The generalized stage curves of the turbofan compressor stages 1 and 2 are shown in figure 3(a). Figure 3(b) shows the turbofan compressor performance map obtained from the generalized stage curves of figure 3(a) and reference 9, the specified design information, and the stacking procedure discussed in reference 10.

The full-power operating lines on the fan and compressor maps of the turbofan engine are shown in figure 2(b) and 3(b). These lines result from matching engine components for the assigned full-power operating mode in which engine mechanical speed and turbine-inlet temperature are held constant at their design values. Engine operation at design equivalent speed corresponds to a flight Mach number of 1.28 in the stratosphere, and at 70-percent speed corresponds to Mach 2.95.

### Rotating Stall

Reference 10 estimates that rotating stall will exist up to about 72 percent of design speed for the modified eight-stage compressor. In the reference, a line representing first-stage operation at the flow coefficient corresponding to maximum first-stage equivalent total-pressure ratio was located on the predicted compressor performance map. Compressor operation to the left of this line corresponds to stalled

operation of the first stage. The actual performance of the modified
eight-stage compressor is discussed in reference 12. Three- and four-
zone rotating-stall patterns were indicated up to equivalent speeds of
approximately 73 percent of design speed (72 percent of design speed was
predicted). Rotating-stall-excited rotor-blade vibratory stresses as
high as ±17,700 psi and stator-blade vibratory stresses as high as
±59,500 psi were recorded. For this analysis, it is assumed that rotat-
ing stall is likely to occur whenever the inlet flow coefficient becomes
less than the value corresponding to maximum equivalent total-pressure
ratio for the inlet stage.

The variation in turbofan compressor and fan inlet flow coefficients
with equivalent speed and flight Mach number is shown in figure 4. The
compressor inlet flow coefficient decreases with decreasing equivalent
speed (increasing flight Mach number). At an equivalent speed of 81-
percent design (Mach 2.27) the inlet stages of the compressor operate at
the flow coefficient for maximum equivalent total-pressure ratio. The
fan inlet flow coefficient behaves quite differently. It increases as
equivalent speed decreases, so that the average fan incidence angle is
always equal to or less than design. Whether or not these conflicting
trends of the compressor and fan will result in rotating stall is exam-
ined by considering the variation of the turbofan inlet flow coefficient
based on the total flow through the fan and the compressor.

In figure 5, the total flow coefficient for both the fan and com-
pressor of the turbofan engine is plotted against equivalent speed and
flight Mach number. Although the total flow coefficient decreases as
flight Mach number increases, even at Mach 2.95 the inlet flow coeffi-
cient is considerably greater than the value corresponding to maximum
first-stage equivalent total-pressure ratio. Thus, although the com-
pressor inlet flow coefficient (for the inner part of the annulus) de-
creases below the value for which rotating stall might be expected, the
total flow coefficient (for the complete annulus) always remains well
above its limiting value because of the high flow through the outer part
of the annulus.

Rotor-blade-row experimental tests were made to determine whether
the limit for rotating stall would be set by the average flow coeffi-
cient for the complete annulus or by compressor flow coefficient for
the inner part of the annulus. These tests indicated that the limiting
value of inlet flow coefficient for the complete annulus (below which
rotating stall is present) decreases as more and more airflow is forced
through the outer part of the annulus. The maximum decrease attained
during the tests was about 7 percent. This trend would lower the stall
limit in figure 5 at high flight Mach numbers and therefore further de-
crease the probability of encountering rotating stall in the turbofan
engine. Thus, rotating stall is not likely to be encountered in a
turbofan engine with conventional compressor designs. If the turbofan

engine had an unconventional compressor design in which stall occurred at the hub, this conclusion probably would not be valid.

Turbofan Inlet Axial Velocity

The assumption regarding the division of flow between the turbofan fan and compressor results in sizable differences between the fan and compressor average inlet axial velocities (fig. 6(a)). The ratio of fan to compressor average axial velocity increases from 1.00 at Mach 1.28 to 1.63 at Mach 2.95 (fig. 6(b)).

The results of the experimental tests on the single rotor-blade row were inconclusive with regard to inlet axial velocity variations. The data obtained at 60-percent design speed with and without inner-annulus additional throttling are shown in figure 7. In figure 7(a) mass flow per unit flow area at station b (midway between the trailing edge of the rotor blades and the leading edge of the cylindrical annulus divider) is plotted against radius at station b. The weight flow for each run was slightly greater than the weight flow below which rotating stall normally exists. Operation with additional inner-annulus throttling resulted in a shift of flow from the inner to the outer annulus. The ratio of flow per unit flow area with inner-annulus throttling to that without inner-annulus throttling is plotted against radius at station b in figure 7(b). Without inner-annulus throttling the ratio of outer-annulus weight flow to inner-annulus weight flow is 0.66. With inner-annulus throttling, the ratio increased to 0.96.

The effect of this large radial shift in mass flow downstream of the rotor on the inlet axial velocity is shown in figure 7(c), where the ratio of inlet axial velocity with inner-annulus throttling to inlet axial velocity without inner-annulus throttling is plotted against inlet radius. The maximum increase in inlet axial velocity in the outer part of the annulus is about 2.5 percent. The trend could have been expected, but the small increase in outer-annulus axial velocity is not necessarily representative of the increase in an actual turbofan engine. The flow conditions for the experimental data do not simulate the flow conditions that would exist along the full-power operating line of a turbofan engine. The experimental data with inner-annulus throttling are for a ratio of inlet flow coefficient to design inlet flow coefficient of 0.56 and a ratio of outer- to inner-annulus mass flow of 0.96. For the turbofan of this report, the former ratio varies along the full-power operating line from 1.0 to 0.91, and the latter ratio from 1.46 to 2.27.

CU-2

## Weight-Flow Variations

A high turbofan weight flow at equivalent speeds less than design results from the fan characteristics and the position of the full-power operating line on the fan performance map (fig. 2(b)). The fan, being a low-pressure-ratio unit, passes relatively more flow at all equivalent speeds less than design than does the higher-pressure-ratio turbofan compressor. At 70-precent speed and maximum efficiency, for example, the fan passes about 76 percent of its design weight flow (fig. 2(b)) compared with about 52 percent for the turbofan compressor (fig. 3(b)). Thus, if the full-power operating lines on the fan and compressor maps follow the maximum-efficiency lines, the fan relative weight flow would be considerably higher than the compressor relative weight flow for the higher supersonic flight Mach numbers. The fan weight-flow advantage is even more pronounced because the full-power operating line on the fan map lies on the high-weight-flow side of the maximum-efficiency line (fig. 2(b)), whereas the operating line of the turbofan compressor (fig. 3(b)) tends to follow the maximum-efficiency line.

The variation of turbofan weight flow with flight Mach number is shown in figure 8. At Mach 2.95 (70 percent of equivalent design speed) the turbofan weight flow is 68.5 percent of its design value (fig. 8(a)). The turbofan fan and compressor weight flows relative to their design values are compared in figure 8(b). The turbofan compressor weight-flow variation is about what could be expected for the compressor of a turbojet engine having the same design compressor total-pressure ratio as the turbofan engine. At Mach 2.95, compressor weight flow is only 51.5 percent of its design value. A turbojet engine with a lower design total-pressure ratio would pass more weight flow, but only a very low design total-pressure ratio would result in a weight-flow variation approaching that of the turbofan engine. For the turbofan engine of this analysis, then, at Mach 2.95 the turbofan passes about 33 percent more airflow than would a turbojet of about the same design compressor total-pressure ratio. This compares with about a 25-percent turbofan weight-flow advantage at Mach 3.0 predicted in other analyses where fan performance is assumed to be that which would be obtained from testing the fan as a separate component.

## CONCLUDING REMARKS

The variation of turbofan inlet flow coefficient based on total flow with flight Mach number (or equivalent speed) indicates that turbofan flow would be free of rotating stall. The experimental tests on a single rotor-blade row rigged to simulate turbofan operation indicated a favorable trend with regard to rotating-stall limits. The inlet flow coefficient below which rotating stall exists was found to decrease as more and more airflow was forced through the outer annulus.

Turbofan weight flow at part speed was high. At 70 percent design speed, it was 68.5 percent of its design value. This is much higher (about 33 percent) than the weight flow attainable in a turbojet engine having a comparable design compressor total-pressure ratio.

Lewis Flight Propulsion Laboratory
  National Advisory Committee for Aeronautics
    Cleveland, Ohio, August 12, 1957

APPENDIX - SYMBOLS

A        area, sq ft

a,b,c    constants in eq. (4)

f        function

H        stagnation enthalpy, Btu/lb

M        Mach number

N        rotational speed, rpm

P        total pressure, lb/sq ft

p        static pressure, lb/sq ft

r        radius, ft

T        total temperature, °R

U        rotor speed, ft/sec

V        air velocity, ft/sec

w        weight flow, lb/sec

β        flow angle, measured from axial direction, deg

γ        ratio of specific heat at constant pressure to specific heat at
         constant volume

δ        ratio of total pressure to NACA standard sea-level pressure of
         2116 lb/sq ft

η        adiabatic efficiency

θ        ratio of total temperature to NACA standard sea-level temperature
         of 518.7° R

ρ        density, lb/cu ft

Subscripts:

A,B,C    turbofan stations:  fan inlet, fan outlet, and duct outlet
         (see fig. 1)

4319

an        annular

b         experimental rotor blade exit

c         compressor

d         design

eq        equivalent

f         fan

m         mean

n         stage number

t         tip

th        throttling in inner annulus

z         axial

0         ambient

1         compressor inlet

2'        outlet of second compressor stage

2         combustor inlet

3         turbine inlet

4         turbine outlet

5         turbine diffuser outlet

6         exhaust-nozzle inlet

Superscript:

'         relative to rotor


# REFERENCES

1. Mallett, William E., and Groesbeck, Donald E.:  Effects of Compressor
      Interstage Bleed and Adjustable Inlet Guide Vanes on Compressor
      Stall Characteristics of a High-Pressure-Ratio Turbojet Engine at
      Altitude.  NACA RM E55G27, 1955.

4319

2. Huntley, S. C., Huppert, Merle C., and Calvert, Howard F.: Effect of Inlet-Air Baffles on Rotating-Stall and Stress Characteristics of an Axial-Flow Compressor in a Turbojet Engine. NACA RM E54G09, 1955.

3. Calvert, Howard F., Medeiros, Arthur A., and Johnson, Donald F.: Effect of Inlet-Guide-Vane Angle on Blade Vibration and Rotating Stall of 13-Stage Axial-Flow Compressor in a Turbojet Engine. NACA RM E55K03, 1956.

4. Wallner, Lewis E., and Lubick, Robert J.: Steady-Stage and Surge Characteristics of a Compressor Equipped with Variable Inlet Guide Vanes Operating in a Turbojet Engine. NACA RM E54I28, 1955.

5. Hensley, Reece V., Behun, Michael, and Kerrebrock, Jack L.: An Analysis of the Ducted Fan Engine Cycle. Preprint No. ATI-144 351, Inst. Aero. Sci., 1952.

6. Gist, W. B., Kelber, C. C., Thurlo, M., and Woodworth, L. R.: Performance, Weight, and Size Relations for a Family of Turbofan Engines with Exhaust Mixing. Rep. R-269, Rand Corp., Santa Monica (Calif.), June 30, 1954.

7. Bridle, E. A.: Assessment of the Relative Performance of the By-Pass Engine and the Orthodox Double Compound Jet Engine. R & M No. 2862, British ARC, July 1948.

8. Moak, Harold, and Sievers, Alwin G.: Turbofan Engine Study. Pt. II. WTF4 and WTF6 Performance Analysis. WADC TR 55-288, Wright Air Dev. Center, Wright-Patterson Air Force Base, May 1955.

9. Voit, Charles H., and Geye, Richard P.: Investigation of a High-Pressure-Ratio Eight-Stage Axial-Flow Research Compressor with Two Transonic Inlet Stages. III - Individual Stage Performance Characteristics. NACA RM E54H17, 1954.

10. Geye, Richard P., and Voit, Charles H.: Investigation of a High-Pressure-Ratio Eight-Stage Axial-Flow Research Compressor with Two Transonic Inlet Stages. IV - Modification of Aerodynamic Design and Prediction of Performance. NACA RM E55B28, 1955.

11. Stodola, A.: Steam and Gas Turbines. Vol. I. McGraw-Hill Book Co., Inc., 1927. (Reprinted, Peter Smith (New York), 1945, p. 222.)

12. Standahar, Raymond M., Hanson, Morgan P., and Geye, Richard P.: Investigation of a High-Pressure-Ratio Eight-Stage Axial-Flow Research Compressor with Two Transonic Inlet Stages. VI - Over-All Performance, Rotating Stall, and Blade Vibration at Low and Intermediate Compressor Speeds. NACA RM E55I13, 1955.
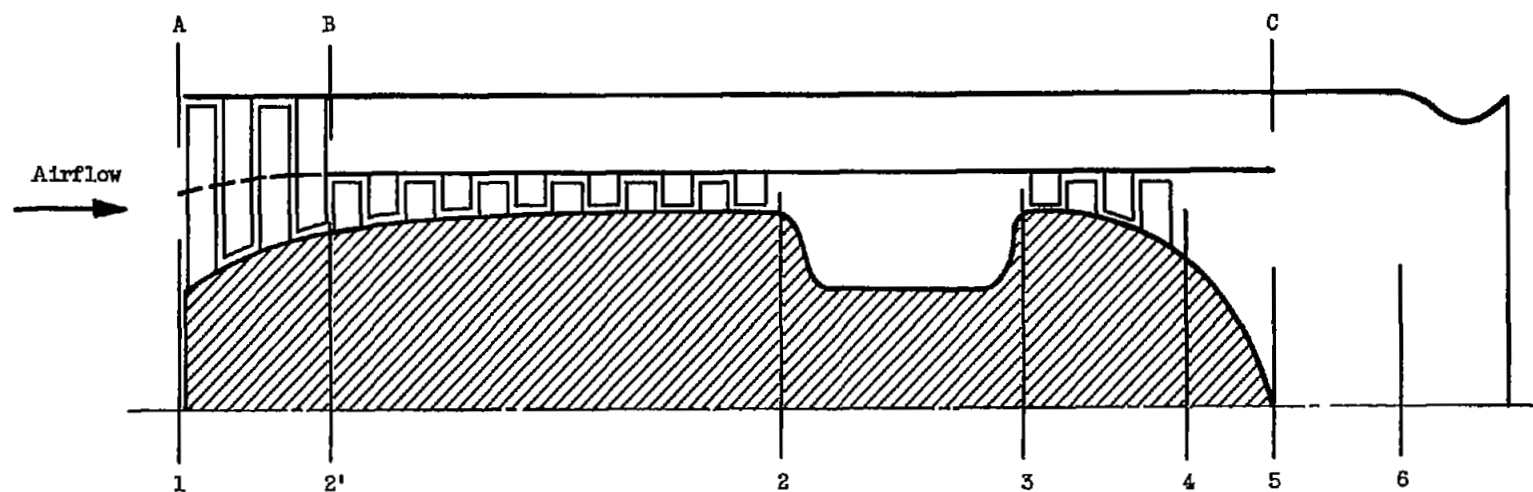
Figure 1. - Cross section of turbofan engine.

CD-5796
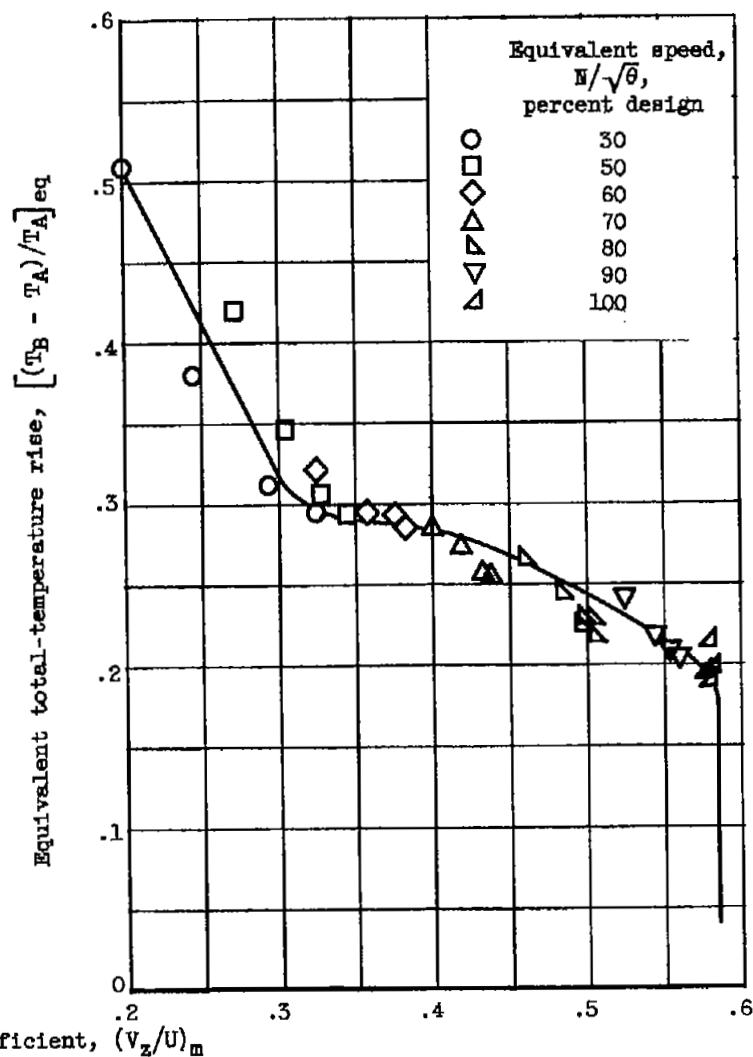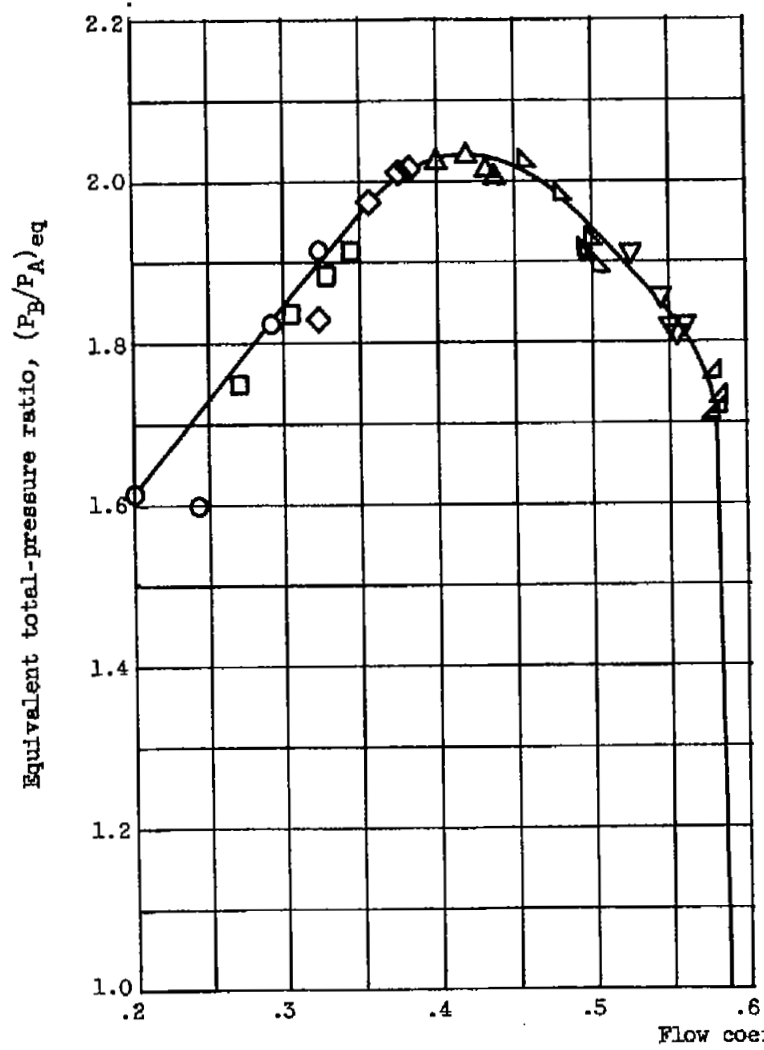
(a) Generalized curves.

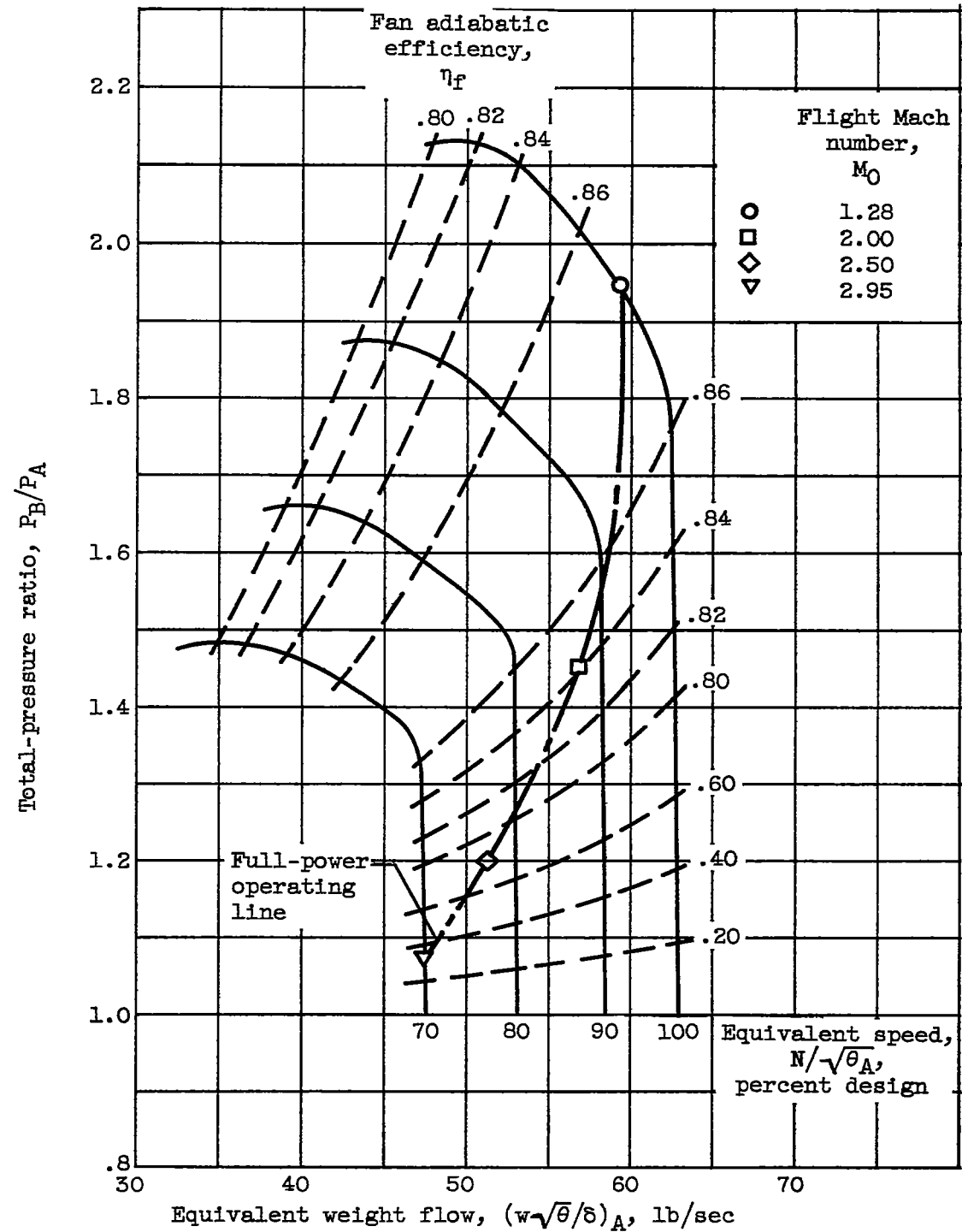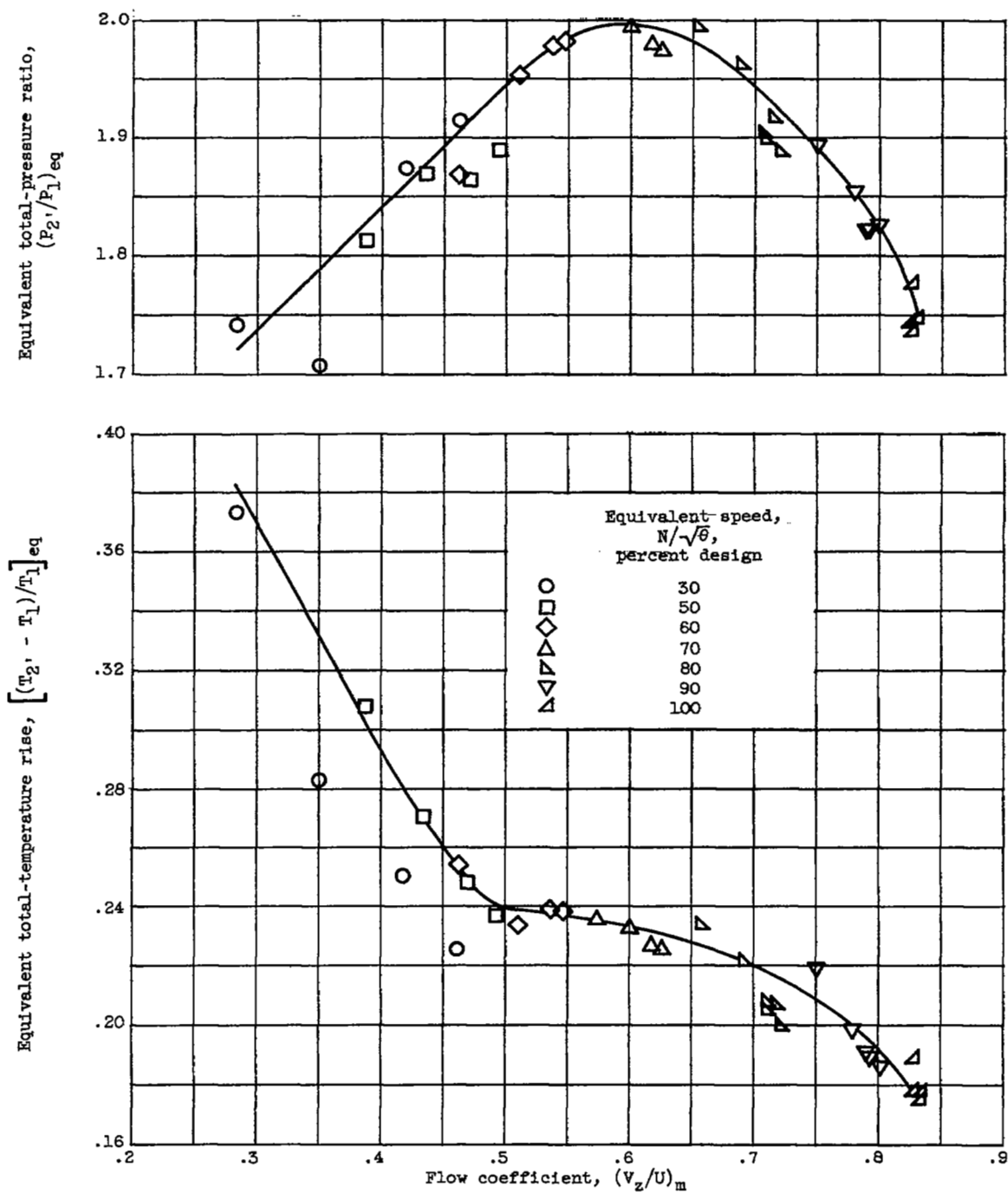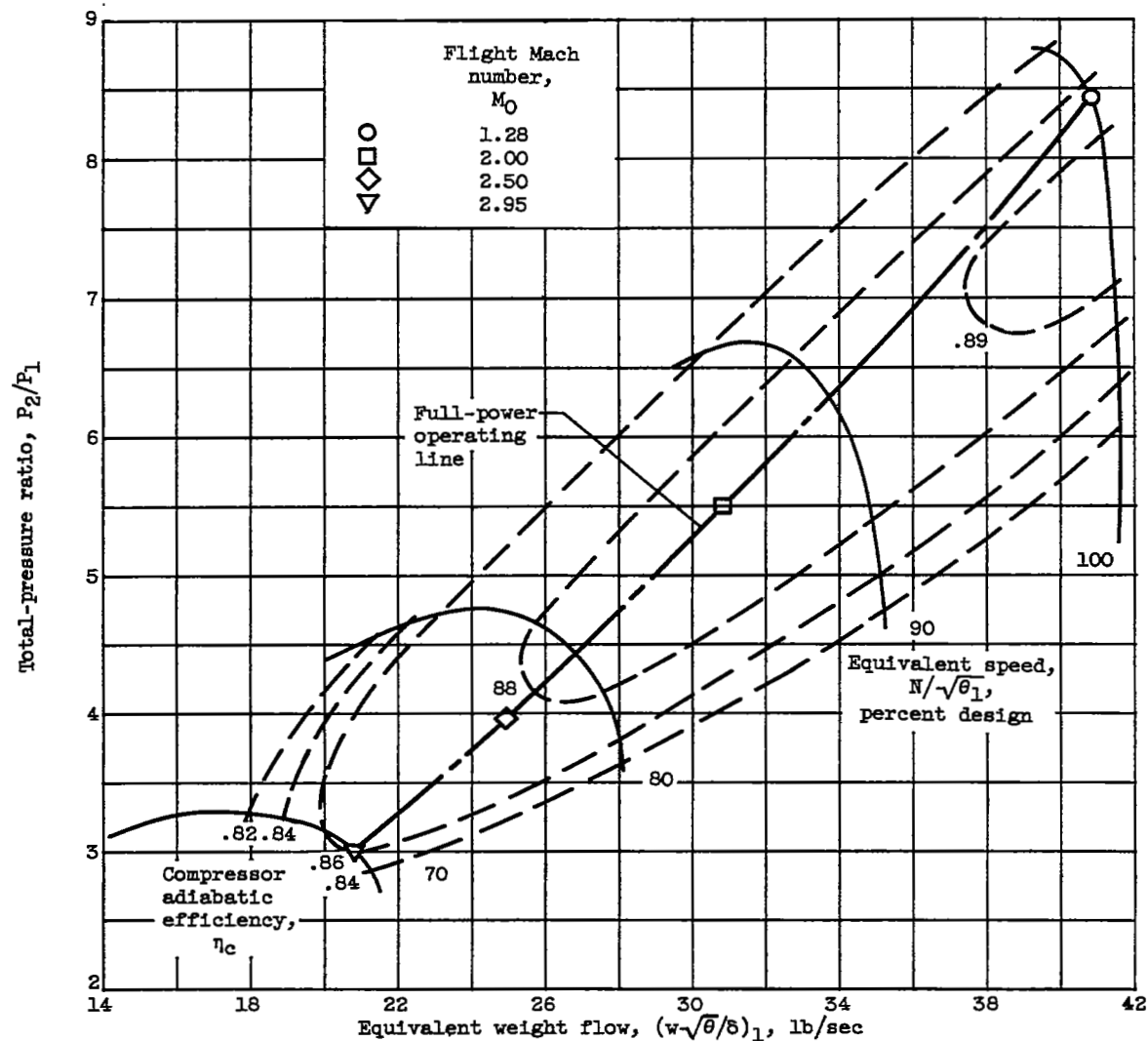Figure 2. - Turbofan fan performance.

(b) Performance map.

Figure 2. - Concluded.  Turbofan fan performance.

(a) Generalized stage curves of turbofan compressor stages 1 and 2.

Figure 3. - Turbofan compressor performance.

CU-3 back                                                                        4319



(b) Performance map.
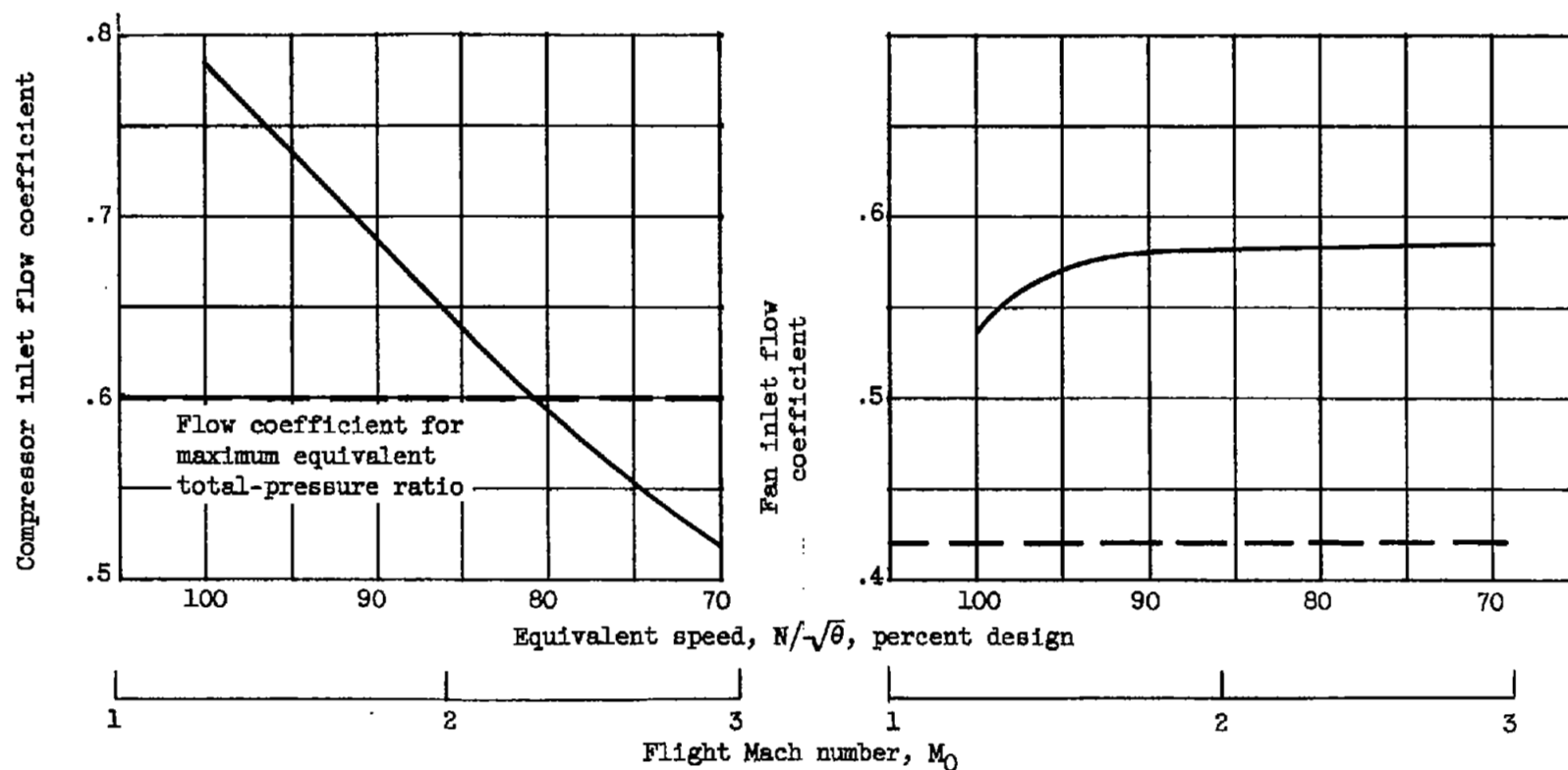
Figure 3. - Concluded.  Turbofan compressor performance.

Figure 4. - Variation of turbofan compressor and fan inlet flow coefficients with equivalent speed and flight Mach number.

4319.
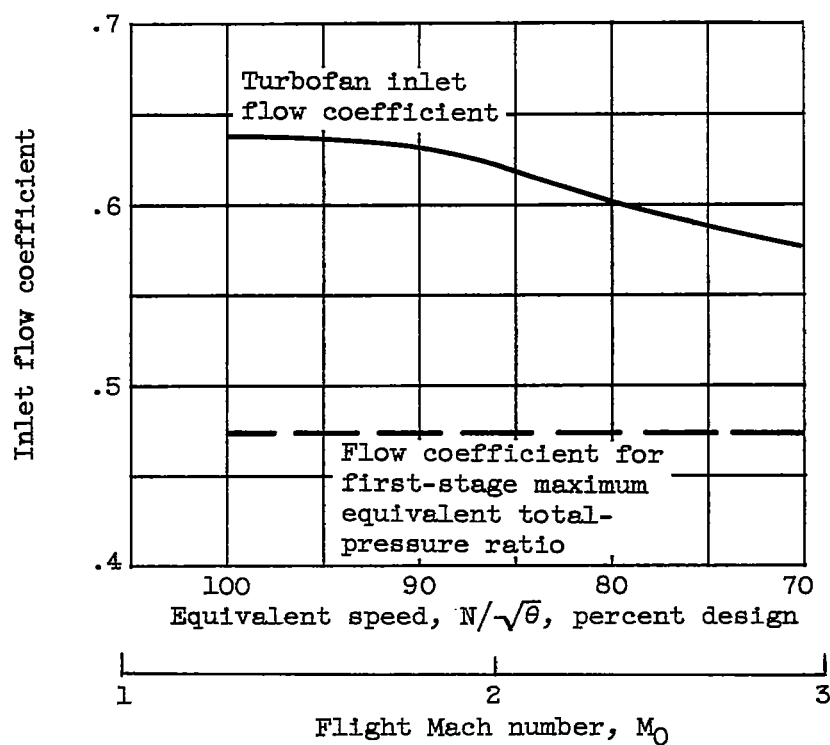


Figure 5. - Variation of turbofan inlet flow
  coefficient with equivalent speed and flight
  Mach number.
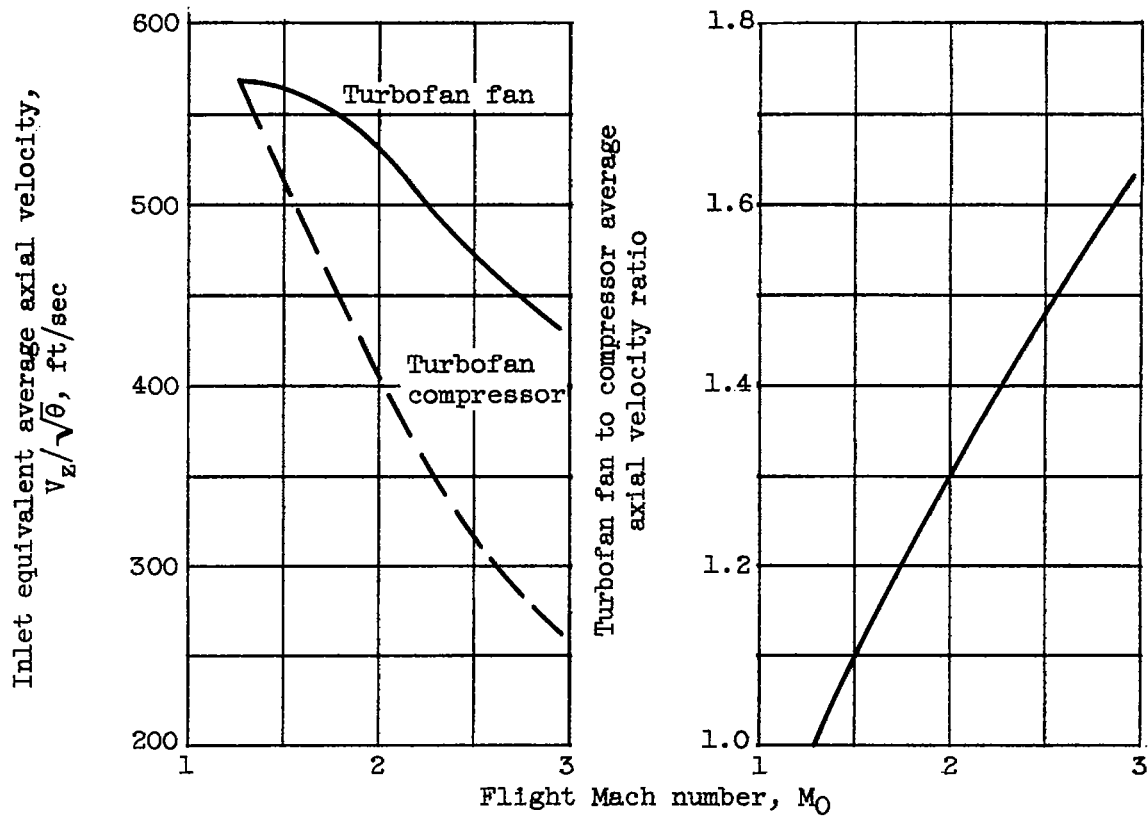
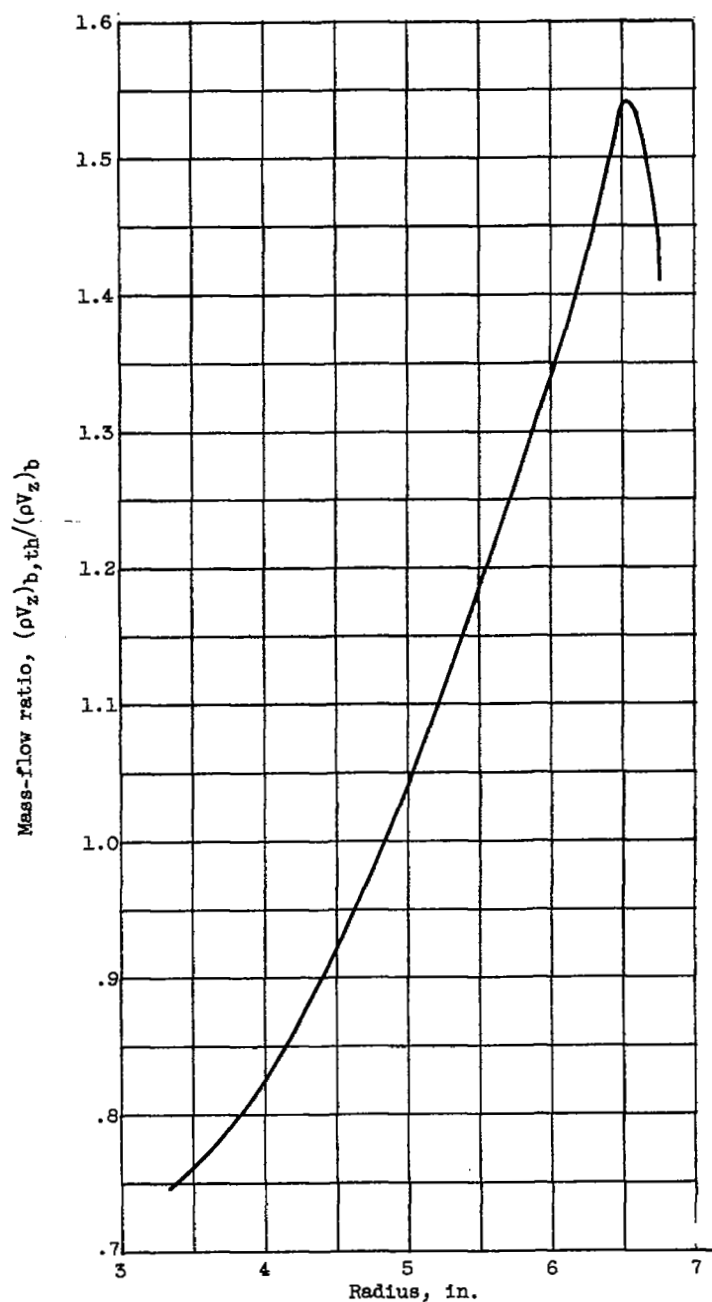(a) Absolute variation.          (b) Relative variation.

Figure 6. - Variation of turbofan fan and compressor average
    axial velocity with flight Mach number.

4319
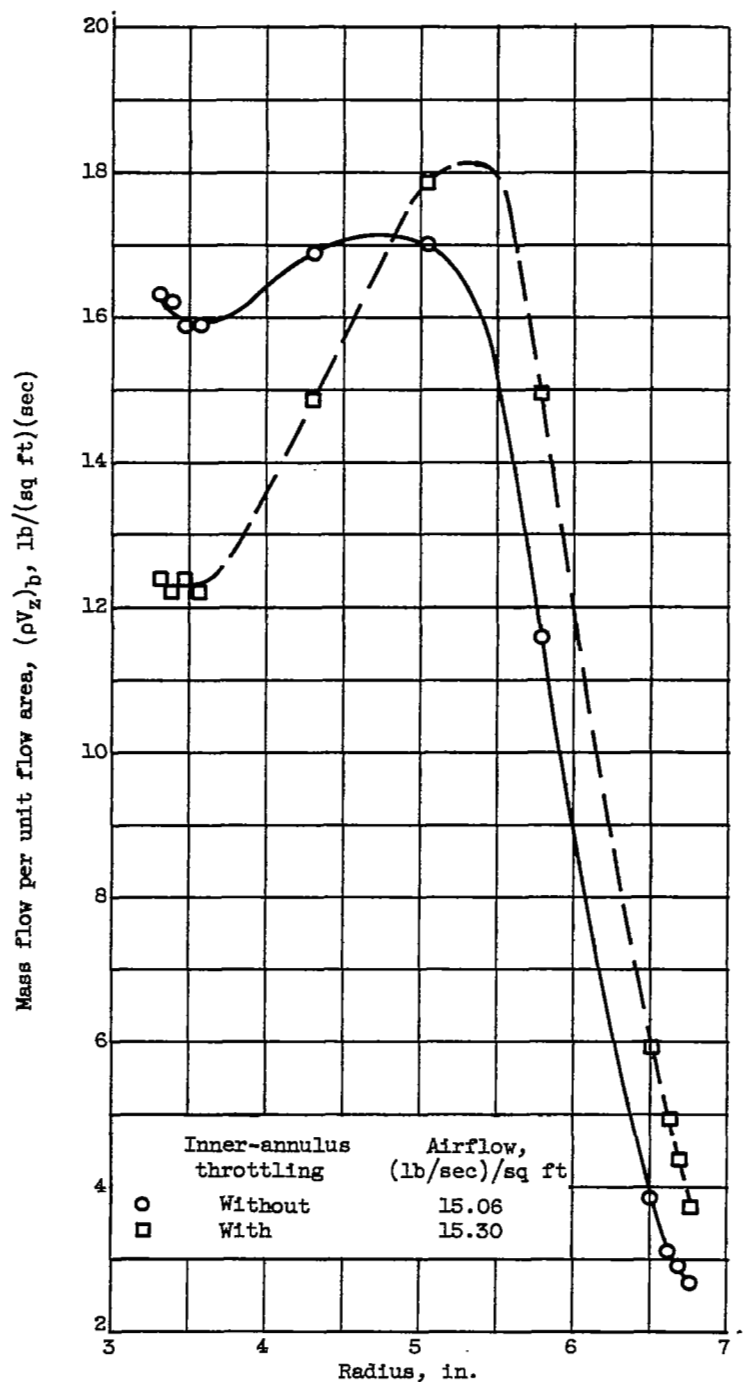


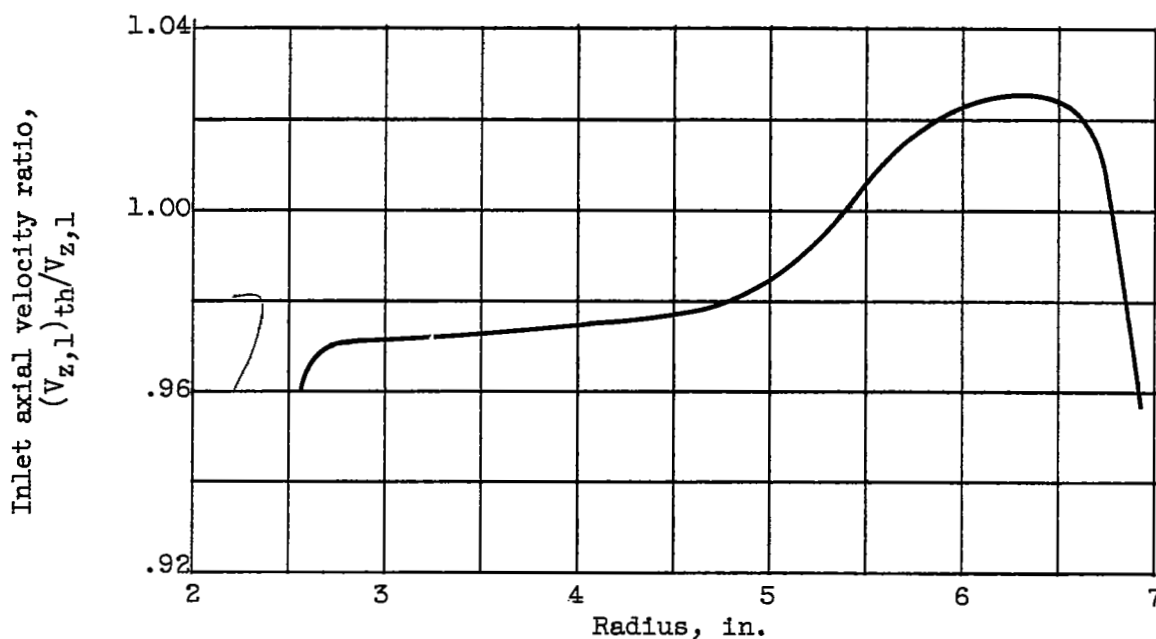(a) Radial variation of mass flow per unit flow area at station b.

Figure 7. - Experimental data from a rotor-blade row operated with and without inner-annulus throttling. Equivalent speed, 60-percent design.

(b) Radial variation of ratio of mass flow per unit
flow area with inner-annulus throttling to that
without at station b. (Airflow with throttling,
15.30 (lb/sec)/sq ft; without, 15.06 (lb/sec)/sq ft.)

Figure 7. - Continued. Experimental data from a
rotor-blade row operated with and without inner-
annulus throttling. Equivalent speed, 60-percent
design.

(c) Radial variation of ratio of inlet axial velocity with
    inner-annulus throttling to that without.  (Aiflow with
    throttling, 15.30 (lb/sec)/sq ft; without, 15.06
    (lb/sec)/sq ft.)

Figure 7. - Concluded.  Experimental data from a rotor-blade
    row operated with and without inner-annulus throttling.
    Equivalent speed, 60-percent design.
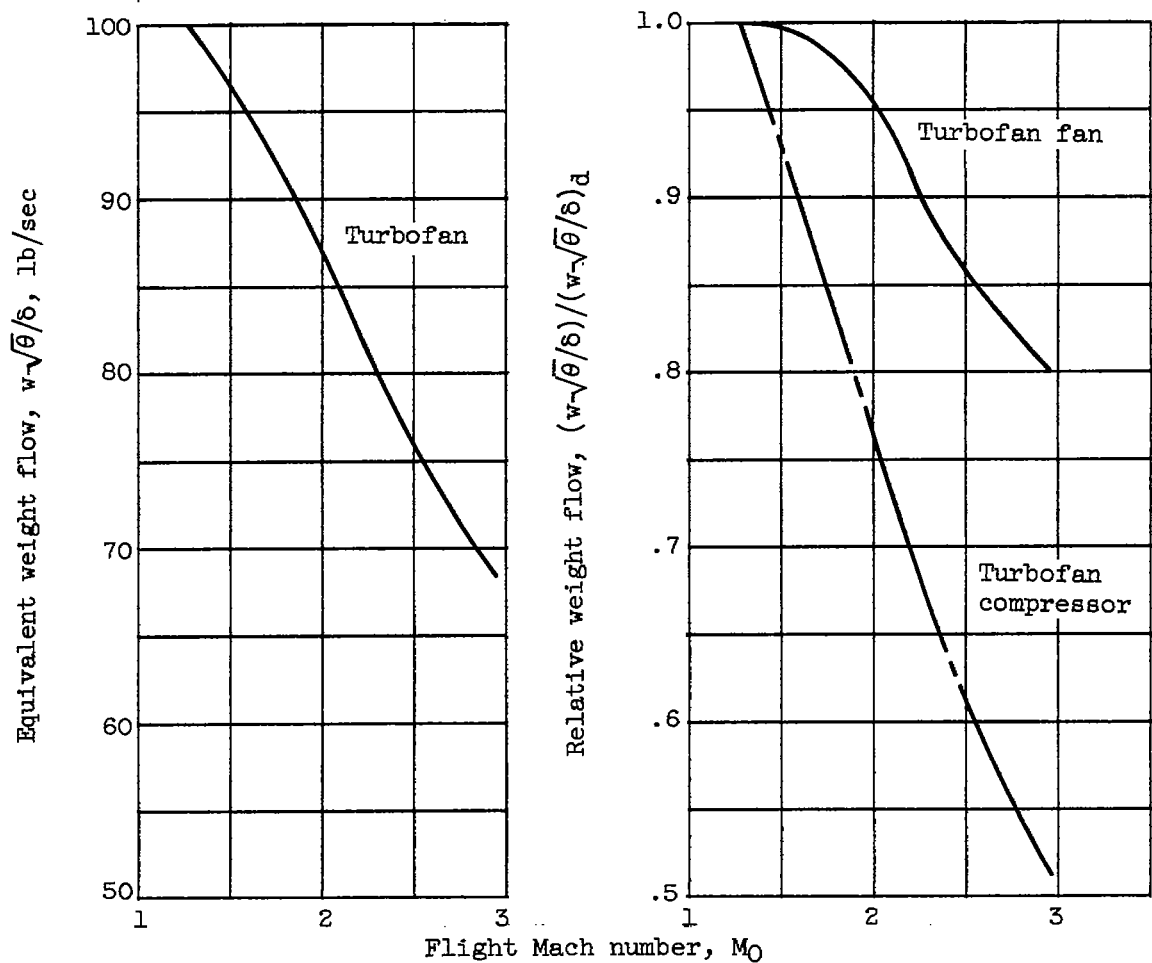
(a) Turbofan weight flow.

(b) Turbofan fan and compressor relative weight flow.

Figure 8. - Turbofan weight-flow variations.